ISSN 2075-1133, Inorganic Materials: Applied Research, 2024, Vol. 15, No. 3, pp. 851–865. © Pleiades Publishing, Ltd., 2024.
Russian Text © The Author(s), 2023, published in Fizika i Khimiya Obrabotki Materialov, 2023, No. 3, pp. 44–62.

NEW METHODS OF TREATMENT AND PRODUCTION OF MATERIALS WITH REQUIRED PROPERTIES

Structure of Alloys for (Sm, Zr)(Co, Cu, Fe)$_z$ Permanent Magnets and Formation Mechanism of High-Coercivity State

A. G. Dormidontov[a, *], N. B. Kolchugina[a, b], N. A. Dormidontov[a, b], P. A. Prokofev[b], M. V. Zheleznyi[a, b], Yu. V. Milov[a, **], A. S. Andreenko[a], I. A. Sipin[a], A. S. Bakulina[b, *], and A. A. Telitsa[a]**

[a] *LLC Magnetoelectromechanics, Moscow, 123458 Russia*

[b] *Baikov Institute of Metallurgy and Materials Science, Russian Academy of Sciences, Moscow, 119334 Russia*

**e-mail: doremi.andr@gmail.com*

***e-mail: milov.yv@mail.ru*

****e-mail: annbak@mail.ru*

Received November 13, 2022; revised March 10, 2023; accepted April 10, 2023

Abstract—Contemporary research methods are used to study in detail the structure and phase composition of the (Sm, Zr)(Co, Cu, Fe)$_z$ alloys with z = 5.5–7.0 in the as-cast state and after heat treatment, which includes the solid-solution treatment at 1150–1180°C for 5 h, subsequent water quenching, isothermal aging at 800°C for 20 h, and cooling (stepped aging) from 800 to 400°C at an average rate of 100°C/h. The transformation scheme of boundary structural constituent of a (Sm, Zr)(Co, Cu, Fe)$_z$ permanent magnet manufactured by powder metallurgy technology is proposed for different heat treatment stages. The formation mechanism of the high-coercivity state of a permanent magnet in the course of complete cycle of heat treatments is given in the form of a sequence of phase transformations accompanied by the redistribution of a number of constituents of the (Sm, Zr)(Co, Cu, Fe)$_z$ alloy.

Keywords: (Sm, Zr)(Co, Cu, Fe)$_z$ permanent magnets, high-coercivity state, heat treatment, boundary phase, phase transformations

DOI: 10.1134/S2075113324700291

INTRODUCTION

Rare-earth metal alloys with transition metals (R–TM) a long time and thoroughly hold the primacy among materials used for manufacturing permanent magnets owing to the unique combination of the high saturation magnetization and magnetic anisotropy. Currently, 99% commercial R–TM magnets is produced on the basis of three types of compositions, namely, $SmCo_5$, (Sm, Zr)(Co, Cu, Fe)$_z$, and Nd–Fe–B, the beginning of the industrial application of which comes from 1969, 1977, and 1985, respectively [1, 2].

The $SmCo_5$ compound was the base of the first R–TM alloys for manufacturing rare-earth permanent magnets, which until now have been used in a number of industrial products.

Today, Nd–Fe–B-based permanent magnets hold the commercial lead in the rare-earth magnet class because of the record magnetization, relatively low cost, and availability of base starting constituents. However, their application is related to a number of limitations. In particular, because of the not high Curie temperature of the $Nd_2Fe_{14}B$ compound ($T_C \approx$ 310°C), the range of operating temperatures of such magnets is limited to an upper limit of 100°C; for compositions alloyed with Dy and/or Tb and Co, the range is limited to an upper limit of 200°C. In this case, peculiarities of the phase composition and high affinity of Ne-rich phases for hydrogen and oxygen determines the necessity of high-quality corrosion protection of the magnets during operation.

Permanent magnets based on samarium–cobalt compositions alloyed with copper, iron, and zirconium, namely, (Sm, Zr)(Co, Cu, Fe)$_z$, because of their unsurpassed combination of the temperature stability and corrosion resistance under external action conditions, are widely used in devices operating at high temperatures, in the most important constructions of aerospace engineering and military equipment, and in traction motors of transport engineering as well. The stability of hysteretic parameters of these magnets is primarily due to the phase composition and structure of the (Sm, Zr)(Co, Cu, Fe)$_z$ alloys.

Since the development and until now, the features of the structural morphology of the (Sm, Zr)(Co, Cu, Fe)$_z$ magnets and, therefore, the phase transformations in the course of treatment of the alloys for the high-coercivity state have attracted the attention of specialists.

The structure of the hard magnetic (Sm, Zr)(Co, Cu, Fe)$_z$ alloys forms by means of a number phase transformations realized as a result of combination of heat treatments, namely, solid solution treatment, quenching, and isothermal and stepped aging (or aging in the course of slow cooling). As a result, a periodic nanostructure ensuring the efficient coercivity mechanism is formed, namely, pinning of domain walls at interphase surfaces [1, 2].

The structural morphology of the (Sm, Zr)(Co, Cu, Fe)$_z$ alloys in the high-coercivity state is carefully investigated and, as a rule, does not cause differences of opinion among specialists. The phase composition of the material comprises cells of the phase (with the rhombohedral Th_2Zn_{17}-type structure (R-3m) in the form of hexagonal bipyramids with the height arranged along to the easy magnetization axis with a period of 60–200 nm (in accordance with the material composition and heat treatment). The cells are separated by a continuous network of phase coherent with the cell phase but having the hexagonal $CaCu_5$-type lattice ($P6/mmm$) and forming boundaries between cells 6–20 nm in thickness (boundary phase). In turn, the entire cell-boundary solid mass is permeated by thin extended Z-phase plates (lamellas) (with the Be_3Nb-type structure, R-3m) 2–4 nm in thickness, which, in turn, is coherent with the boundary and cell phases [3].

Relative to the integral composition of the alloy, the cell phase is depleted in Sm, Zr, and Cu and enriched in Fe and has the maximum volume fraction in the material structure. In turn, the boundary phase is enriched in Sm and Cu but depleted in Fe and Zr. The platelike phase is the primary zirconium acceptor [3, 4].

Upon magnetization reversal, the phase composition of the alloy in the high-coercivity state ensures an efficient mechanism of coercivity, namely, delayed domain wall motion (pinning) at the interface between cells and boundary phase or within boundary phase. The intrinsic coercive force is due to the high gradient of main magnetic constants in passing through the boundary phase from cell to cell.

Such a mechanism of coercivity is confirmed with real samples of (Sm, Zr)(Co, Cu, Fe)$_z$ magnets, magnetization curves, major and minor hysteresis loops, corresponding calculated micromagnetic models, and direct observation of domain walls in using Lorentz microscopy [2–6]. In this case, in fact, the formation mechanism of the high-coercivity phase state of the (Sm, Zr)(Co, Cu, Fe)$_z$ alloys, i.e., the phase transformations realized in the course of heat treatment, are still subject to dispute of specialists.

Two competitive models of phase transformations of the (Sm, Zr)(Co, Cu, Fe)$_z$ alloys in the course of heat treatment were developed. The earlier approach is based on the Ray's metallurgical model [7], which assumes the decomposition of solid solution in the course of isothermal annealing with the formation of phases directly represented in the high-coercivity state of alloy [4–7]. It is alleged that, when stepped aging (or slow cooling) is performed, any transformations are absent, and the increase in the coercive force is reached exclusively by means of redistribution of elements between phases because of temperature dependences of the solubility of these elements in already formed phases. In this case, in contrast to the initial version [7], after homogenizing annealing and quenching, the starting phase is the supersaturated solid solution based on the disordered phase with the $TbCu_7$-type structure ($P6/mmm$) [2–5].

The other variant of the model of formation of the high-coercivity state assumes the same initial structural state before aging (1:7 phase). In the course of isothermal annealing, it is assumed the formation of addition phases belonging to the homologous series (Sm, Zr)$_{n-1}$(Co,Cu,Fe)$_{5n-1}$, such as 2:7 and 5:19 [3, 8–12] as the intermediate structural constituents (between cells). In turn, in the course of stepped (or slow) cooling, within the boundary constituent, the 1:5 boundary phase forms instead of 2:7 and 5:19 phases owing to diffuse exchange of elements and in accordance with variable solubility curves, and it occupies the entire volume between cells.

Thus, as in case of the first variant, the final structure of the alloy in the high-coercivity state is the system of phases $2{:}17R + 1{:}5H + Z(1{:}3R)$, where R and H are the rhombohedral and hexagonal polymorphic modifications, respectively [3, 8–13].

Therefore, knowledge of real phase transformations occurring in the material in the course of magnet manufacturing is crucial for the further improvement of technology, compositions of permanent magnets, and, finally, their main functional parameters.

The aim of the present study is to investigate the processes leading to the formation of the high-coercivity state in the (Sm, Zr)(Co, Cu, Fe)$_z$ alloys in the course of specific stages of heat treatment, which is based on the results of combined analysis of published data and the results of our performed studies [14–19].

EXPERIMENTAL

In the course of the work, samples of seven series with the common formula $Sm_{1-x}Zr_x(Co_{1-a-b}Cu_aFe_b)_z$ and compositions given in Table 1 were studied. The studied samples are pseudo-single crystals separated in the form individual grains of ingots and consisting of collinear phases.

The complex heat treatment of the samples was performed in a high-purity argon atmosphere, which included the solid solution treatment at 1180°C for 5 h and subsequent water quenching, isothermal aging at 800°C for 20 h, and cooling (stepped aging) from 800 to 400°C at an average rate of 100°C/h.

Table 1. Chemical composition of experimental $Sm_{1-x}Zr_x(Co_{1-a-b-c}Cu_aFe_b)_z$ alloys

Series	x	a	b	z
1	0.13	0.088	0.210	6.0–6.8
2	0.15	0.088	0.210	6.0–6.8
3	0.17	0.088	0.210	6.0–6.8
4	0.19	0.088	0.210	6.0–6.8
5	0.15	0.075	0.260	6.0–6.8
6	0.13	0.070	0.240	6.1–6.5
7	0.05–0.25	0.088	0.210	5.5–7.0

In the work, we used optical emission mass spectrometry with inductively coupled plasma, X-ray fluorescence spectroscopy, differential thermal analysis, optical quantitative microscopy (Thixomet-Pro software), analysis of transformation of surface domain structures in the course magnetization reversal (Kerr effect), scanning electron microscopy and local electron microprobe analysis, X-ray diffraction analysis and Rietveld refinement, and measurements of major and minor hysteresis loops with a vibrating-sample magnetometer. The preparation of samples and methods of investigation are described in detail in [14–19].

RESULTS

Microstructure of (Sm, Zr)(Co, Cu, Fe)$_z$ Alloys

As is well known, the high hysteretic parameters of (Sm, Zr)(Co, Cu, Fe)$_z$ permanent magnets result from the nanostructural heterogeneity, which ensures an efficient mechanism of coercivity, namely, the domain wall pinning at structural inhomogeneities. The slowed down solidification of alloys, which is required in order to obtain coarse-grained ingots, leads to the well-developed structural elements; this facilitates their identification.

All studied cast samples subjected to slow cooling after solidification are characterized by the qualitatively identical phase composition that is formed on the basis of a number of intermetallic compounds corresponding to the Sm–Co phase diagram; these are 1:3*R*, 2:7*R*, 2:7*H*, 5:19*R*, 1:5*H*, 1:7*H*, and 2:17*R*.

Figure 1a shows balances of base elements in all phases comprising the structure of alloys directly after solidification. The 2:17 and 1:3 phases are primarily solidified and maximally spaced in the alloy volume. The other phases form as the solidification fronts move, as is shown in Fig. 1a, from edge phases 2:17 and 1:3 to central phases 5:19*R* and 2:7*H*. As the stoichiometry of phases changes from 2:17 to 1:3, two main tendencies are obvious; i.e., (a) in phases with a low Zr content, the Co and Fe concentrations markedly decrease, whereas the Sm and Cu concentrations increase, and (b) as the Zr fraction substituted for Sm increases, the total content of Co and Fe abruptly increases at the expense of the decrease in the Cu concentration in phases. The analogous peculiarities are typical also of phase compositions of samples subjected to the heat treatment for the high-coercivity state (Fig. 2); i.e., in the course of phase formation, elements of the Cu–Zr pair, with regard to phases of the Sm–Co system, are antipodes; this already is well known for the Cu–Fe pair.

As x decreases and z increases, all the $Sm_{1-x}Zr_x(Co_{1-a-b}Cu_aFe_b)_z$ alloys exhibit a monotonic increase in the volume fraction of the 2:17 phase; in this case, the volume fractions of the other phases decrease (Fig. 1b). This tendency is reflected in the morphology of the structure at the level of optical microscopy resolutions.

The structure of samples observed with optical magnifications is represented by a superposition of three main structural constituents denoted as *A*, *B*, and *C* (from darkest to brightest structural elements in etched section surfaces, respectively) and having all attributes of phases (Fig. 3a).

The main dendrite-like gray structural constituent *B* is the primary solidified 2:17 phase. Similarly, anisotropic plates of structural constituent *C*, which are almost white in color, extended along the basal plane of sample, and localized in all samples within structural constituent *A*, are formed on the basis of the primary 1:3 phase and 2:7 phase. The other phases, namely, 2:7*H*, 5:19*R*, and 1:5/1:7*H*, form dark gray structural constituent *A*.

As shown in [14], the relationship of volume fractions of constituents *A*, *B*, and *C* in samples of the (Sm, Zr)(Co, Cu, Fe) alloys having the same chemical composition is almost unchanged from the moment of solidification until the end of complete combination of heat treatments. However, within each of the experimental series, as z of the alloy increases, the volume relationships of structural constituents *A* and *B* occu-

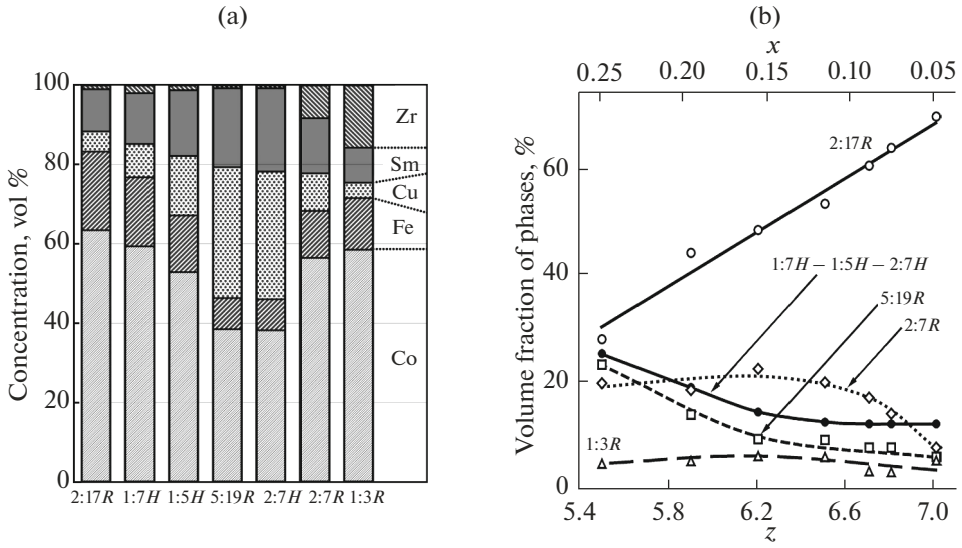

Fig. 1. (a) Contents of main elements in phases and (b) volume fractions (according to X-ray diffraction data and Rietveld refinement) of these phases in the structure of cast alloys of series 7 (Table 1).

pying 85–96% of the total alloy volume monotonically vary from the predominant volume fraction of constituent *A* to predominant volume fraction of constituent *B*. The rest of the volume corresponds to structural constituent *C*, the volume fraction of which monotonically decreases as the content of 3*d* elements (z) increases and increases as x of the $Sm_{1-x}Zr_x(Co,Cu,Fe)_z$ alloy increases.

Thus, the quantitative estimates of tendencies in the behavior of volume fraction of structural constituents *A*, *B*, and *C* and phases formed of them are in full consistency.

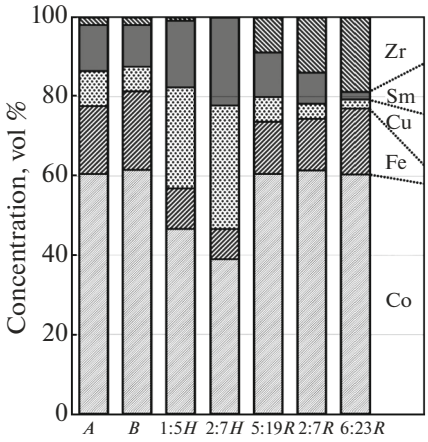

Fig. 2. Contents of main elements (according to electron probe microanalysis data) in phases and main structural constituents *A* and *B* in the $Sm_{1-x}Zr_x(Co_{0.702}Cu_{0.088}Fe_{0.210})_z$ alloys of series 1–5 subjected to complete heat treatment for the high-coercivity state.

Domain Structure of (Sm, Zr)(Co, Cu, Fe)$_z$ Alloys

In the case of the high-coercivity state of samples, the character of the domain structure transformation in each of the main structural constituents *A* and *B* is qualitatively and quantitatively different [15].

The domain structure of constituent *B* and its transformation processes in external magnetic fields are identical to the domain structure and its behavior for (Sm, Zr)(Co, Cu, Fe)$_z$ magnets sintered from fine powders; namely, the magnetization reversal is accompanied by the formation of reverse magnetization domains from numerous centers. In this case, zigzaging domains of submicron width develop, which grow mainly along their largest size. As the negative external field increases, the occupying of the area of the section with reverse magnetization domains occurs by means of adding new domains and densification of the reverse magnetization domain network rather than the increase in their width (Fig. 3b).

The surface domain structure of constituent *A* is identical to that of quasi-binary Sm(Co, Cu)$_z$ and Sm(Co, Cu, Fe)$_z$ alloys with $z = 5–6$. The transformation of the domain structure upon magnetization reversal occurs from limited number of centers with the development of labyrinth domains that transform into fern-shaped domains and widen isotropically in all directions (Fig. 3c).

The maximum local coercivity of domain walls is observed in areas being transition from one to the other structural constituent (*A*–*B*).

Figure 3d demonstrates the effect of monotonic change of the z ratio in the alloys on the change in ranges of the domain wall local coercivity in structural constituents *A* and *B* upon magnetization reversal from the sat-

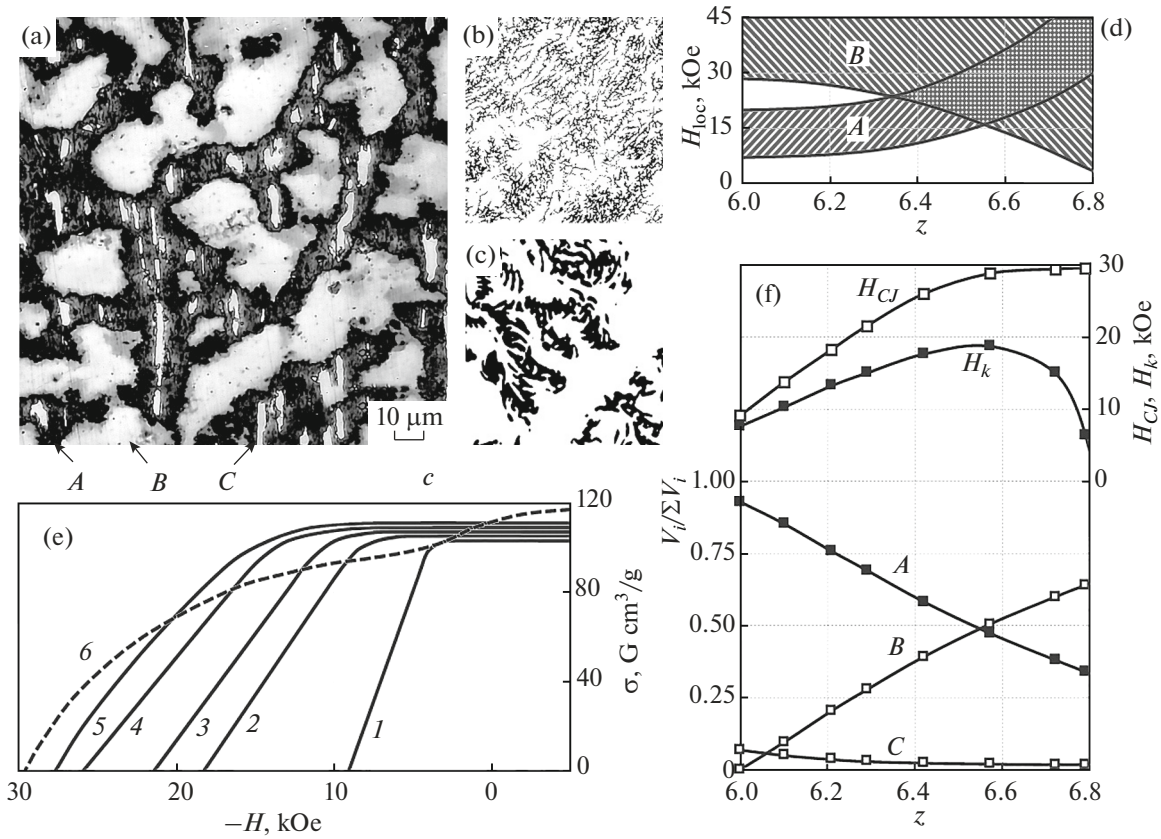

Fig. 3. Correlation between the structure and hysteretic parameters presented by an example of $Sm_{0.85}Zr_{0.15}(Co_{0.702}Cu_{0.088}Fe_{0.210})_z$ alloys: (a) microstructure (prismatic plane) of sample with $z = 6.4$; (b, c) morphology of magnetic domains in structural constituents *B* and *A*, respectively; (d) ranges of local coercivity in structural constituents *A* and *B* upon magnetization reversal of samples from the saturation state; (e) magnetization reversal portions of major hysteresis loops (ignoring the demagnetizing factor $N = 1/3$) at *z* equal to (*1*) 6.0, (*2*) 6.2, (*3*) 6.3, (*4*) 6.4, (*5*) 6.5, and (*6*) 6.8; (f) dependences of volume fractions of structural constituents *A*, *B*, and *C* ($V_i/\Sigma V_i$), coercive force (H_{CJ}), and degree of hysteresis loop squareness (H_k is the field corresponding to $4\pi J = 0.94\pi J_S$) on the chemical composition *z*.

uration state of $Sm_{0.85}Zr_{0.15}(Co_{0.702}Cu_{0.088}Fe_{0.210})_z$ experimental samples after the complete heat treatment cycle. As *z* increases, the values of the top and bottom limits of the range of domain wall local coercivity in structural constituent *A* and *B* increase and decrease, respectively.

Hysteretic Properties of Pseudo-Single-Crystal (Sm, Zr)(Co, Cu, Fe)$_z$ Samples

Figure 3e shows the magnetization reversal portions of major hysteresis loops of $Sm_{0.85}Zr_{0.15}(Co_{0.702}Cu_{0.088}Fe_{0.201})_z$ samples with z = 6.0, 6.2, 6.3, 6.4, 6.5, and 6.8. The majority of shown magnetization reversal curves correspond to major hysteresis loops; i.e., the condition $(BH)_{max} = (4\pi J_S)^2/4$ is satisfied, where $(BH)_{max}$ is the maximum magnetic energy product and J_S is the spontaneous saturation magnetization. As *z* increases, the coercive force of the pseudo-single-crystals monotonically increases in the whole concentration range under study. However, from a certain moment, in a range of low external field, a "shoulder" appears on the magnetization reversal curve; i.e., the hysteresis loop squareness worsens.

Such a behavior is absolutely typical of samples of all series of alloys. The difference consists only in the value of the "shoulder." The lower the relative zirconium concentration (*x*), the clearer the "shoulder." Moreover, as the relative zirconium concentration (*x*) increases, the *z* values of alloy at which the worsening of the loop squareness manifests itself shifts to lower values.

Correlations between the Structure and Hysteretic Characteristics of (Sm, Zr)(Co, Cu ,Fe)$_z$ Alloy Samples

The volume fractions of structural constituents *A*, *B*, and *C* (V_i), coercive force (H_{CJ}), and hysteresis loop squareness indicator (H_k) corresponding to the external field at which the magnetization of sample decreases to $4\pi J = 0.94\pi J_S$ as functions of the chemi-

cal composition (z) are given in Fig. 3f and are typical of the studied alloys in the high-coercivity state.

The analysis of the dependences allows us to conclude that

(a) the volume fractions of the main structural constituents A and B corresponding to ~90% of the total alloy volume monotonically change from the predominant volume fraction of structural constituent A to the predominant volume fraction of structural constituent B;

(b) as the relative content of 3d elements (z of alloy) and the volume fraction of structural constituent B increase to the alloy compositions at which the equality of volume fractions of structural constituents A and B ($V_A = V_B$) is reached, the active increase in the coercive force is observed; after that, at $V_A < V_B$, the increase in H_{CJ} slows down, and the dependence goes to a horizontal "plateau";

(c) the attainment of the equality of volume fractions of structural constituents A and B ($V_A = V_B$), besides the termination of the increase in H_{CJ}, is accompanied by the appearance of a "shoulder" on the magnetization reversal curves of samples; i.e., when the alloy composition reaches the chemical composition corresponding to the condition $V_A < V_B$, the worsening of the hysteresis loop squareness starts;

(d) the comparison of these functional dependences with those given in Fig. 3d shows that the optimum hysteretic properties of the samples correlate with the equality of lower limits of local domain wall coercivity in structural constituents A and B.

All the functional dependences on the relative Zr content (x) for the $Sm_{1-x}Zr_x(Co, Cu, Fe)_z$ alloys exhibit absolutely identical behavior. The behavior of the volume fraction of structural constituent C is the exception; i.e., as x increases, the volume fraction of structural constituent C naturally increases.

The reported conclusions are valid for all studied series of the $Sm_{1-x}Zr_x(Co, Cu, Fe)_z$ alloys.

Peculiarities of Compositions and Morphology of Main Structural Constituents of (Sm, Zr)(Co, Cu, Fe)$_z$ Alloys in High-Coercivity State

As was already noted, the morphology and character of transformation of domain structures of main structural constituents A and B indicate the different nature of domain wall pinning centers in them; this was shown by studies of the fine structure of the constituents [17].

The heterogeneity of structural constituent A is represented by regular rows of quasi-spherical precipitates less than 50 nm in size. In turn, structural constituent B is represented by coarser morphology, which, by all accounts, is analogous to the known cellular structure of sintered magnets based on (Sm, Zr)(Co, Cu, Fe)$_z$ alloys. Precipitates in structural constituent B are arranged in chevrons that form typical angles of 120° with a period of ~120–140 nm.

In this case, it seems that structural constituent A in passing to B "flows in" spaces between hexagonal bipyramidal cells and forms the boundary phase. In this case, in the A–B transition, precipitates typical of A remain, but near cells forming B, they deform and lose their quasi-spherical shape. Here, it is of importance to note that the magnetization reversal of all pseudo-single crystals starts with the formation of reverse domains in central areas of structural constituents A and B, and the maximum local domain wall coercivity is characteristic of transition areas $A + B$.

Peculiarities of the chemical compositions of main structural constituents A and B and individual phases, which were found in amounts sufficient for the local microprobe analysis exclusively within structural constituents A, are studied for all experimental series of samples in high-coercivity states [17] and, in a generalized form, are given above in Fig. 2.

Structural constituent C, which is present only within A, results from the coalescence of the 5:19R, 2 : 7R, and, likely, 6:23 phases. In turn, the 1:5H and its supersaturated derivative 2:7H were found to result from the coalescence of quasi-spherical precipitates within structural constituent A. Taking into account the above noted "flow in" of structural constituent A in B in the transition region and the rigidity of domain wall pinning in it, just the 1:5H phase is the prototype of the boundary phase separating cells in sintered (Sm, Zr(Co, Cu, Fe)$_z$ magnets. The 2:7H phase could well form as a result of supersaturation of the boundary phase with samarium and copper in ternary junctions of cells.

On the basis of the analysis of compositions and morphology of the main structural constituents of the (Sm, Zr)(Co, Cu, Fe)$_z$ alloys in the high-coercivity state, in [17], a conclusion is made about the common and spatially continuous matrix based on the hexagonal structure described by space group $P6/mmm$ at all stages of heat treatment.

DISCUSSION

Cobalt and samarium, as the base of the (Sm, Zr)(Co, Cu, Fe)$_z$ alloys, ensure the formation of a number of intermetallic compounds at the cobalt end of the Sm–Co phase diagram, which exhibit impressive magnetic parameters and uniaxial anisotropy at room temperature. In turn, the substitution of iron for a part of cobalt allows one to substantially increase the spontaneous saturation magnetization J_S (Table 2) [20, 21].

We clarify the role of the other additions in the formation of the structure of the high-coercivity state of (Sm, Zr)(Co, Cu, Fe)$_z$ alloys.

Table 2. Magnetic parameters of intermetallic compounds based on samarium and cobalt

Compound	Saturation magnetization J_s, T	Saturation magnetization , $K \times 10^{-15}$, J/cm^3	Anisotropy field , H_A, kOe	Curie temperature T_C, °C
Sm_2Co_7	0.77	4.5	>200	~400
$SmCo_5$	1.14	13	350–440	~750
Sm_2Co_7	1.25	4.2	54–107	~920
$Sm_2(Co_{0.7}Fe_{0.3})_{17}$	1.45	3.0	41–64	~840

Role of Zirconium in (Sm, Zr)(Co, Cu, Fe)$_z$ Alloys

The effect of zirconium on the magnetic properties of (Sm, Zr)(Co, Cu, Zr)$_z$-based magnets can be judged by its effect on the magnetic parameters of the 2:17 phase having the predominant volume fraction in the structure of the alloy in the high-coercivity state.

In particular, in the single-phase $Sm_2Co_{17-x}Zr_x$ material, the substitution of Zr for Co in the range $x = 0–1$ leads to the decrease in the Curie temperature by ~95°C/atom and magnetization by ~0.18 T/atom and increase in the anisotropy field by ~46 kOe/atom [22]. The substantial positive effect of substitution of zirconium on the H_A parameter is leveled by, in this case, the decrease in the Curie temperature and, even worse, the substantial decrease in the saturation moment. It is obvious that, with regard to the (Sm, Zr)(Co, Cu, Fe)$_z$ alloys, the main role of zirconium unlikely consists in its effect on the hysteretic properties.

In this specific case, the function of Zr is related to its effect on the modification of phase composition of alloys in the whole range of technological temperatures. Indeed, already very small zirconium additions lead to qualitative changes of equilibria in the Co–Sm system. Already in the ternary Co–Sm–Zr system at high temperatures, a wide region of solid solution based on the disordered phase with the $TbCu_7$-type structure (*P6/mmm*) forms, which is continuous and connects the regions of homogeneity of the 2:17 and 1:5 phases [23–27]. Just the existence of a wide region of homogeneity of the phase with the $TbCu_7$ structure at 1200–1100°C, which decomposes into a number of intermetallic compounds at lower temperatures, ensures the possibility of efficient precipitation magnetic hardening of the (Sm, Zr)(Co, Cu, Fe)$_z$ alloys.

The phase equilibria for the (Sm, Zr)(Co, Cu, Fe)$_z$ alloys in limited composition ranges for the region of existence of the 2:17 phase are given, in particular, in [28–30]. With careful analysis of the partial sections given in these studies, serious inaccuracies in the graphical display of results of these studies become obvious. This is clearly illustrated in Fig. 4, which shows a portion of the quasi-ternary Sm–Zr–(Co, Cu, Fe) phase diagram in the form of two isothermal sections superimposed on each other, which were constructed by us using experimental data of [28–30]. The section at 1160–1185°C shows the region of distribution of supersaturated solid solution based on polymorphic modifications of the 2:17 phase at optimum solid solution heat treatment at 1160–1185°C (region *1* + *2*). The other section at 800°C (region *1*), in accordance with data of [28–30], shows the decrease in the region of homogeneity of the 2:17 phase at 800°C.

Wide black lines show the probable position of the boundary of homogeneity region at 1160–1185°C, which is nearest to the corner of the 3*d* metal (Co, Cu, Fe). Indeed, the region of existence of the high-temperature hexagonal polymorphic modification of the 2:17 phase adjoins just the boundary [28–30]. Just this *H* polymorphic modification of (Sm,Zr)(Co,Cu,Fe)$_{17}$ ensures the substantial widening of the 2:17 phase region upon adding Zr (the substantiation of the position of Zr in formulas of phases in the form of Sm$_n$(Co, Cu, Fe, Zr)$_m$ and (Sm,Zr)$_n$(Co, Cu, Fe)$_m$ is given in [14]). The dense section lining shows the real scale of the existence region of the 2:17 phase, which currently

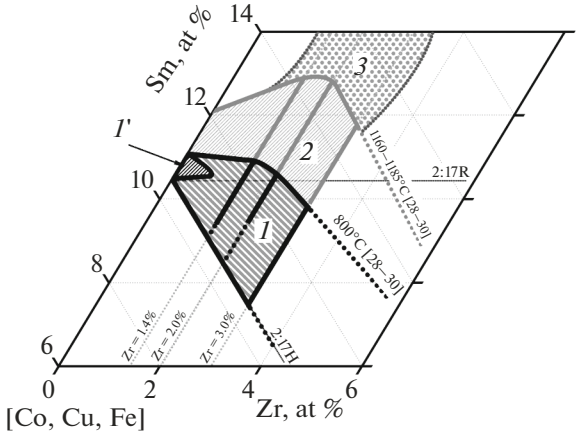

Fig. 4. Transformation of the region of homogeneity of polymorphic modifications 2:17–1:7 for the Sm–Co–7 at % Cu–22 at % Fe–Zr alloy upon cooling from the maximum solubility temperature (1160–1185°C) to 800°C [28–30]: region *1* (800°C); regions *1* + *2* (1160—1185°C); region *3* (phase 1:7 plume between 1185 and 800°C. Region *1*' corresponds to the actual region of homogeneity of the 2:17 phase at 800°C.

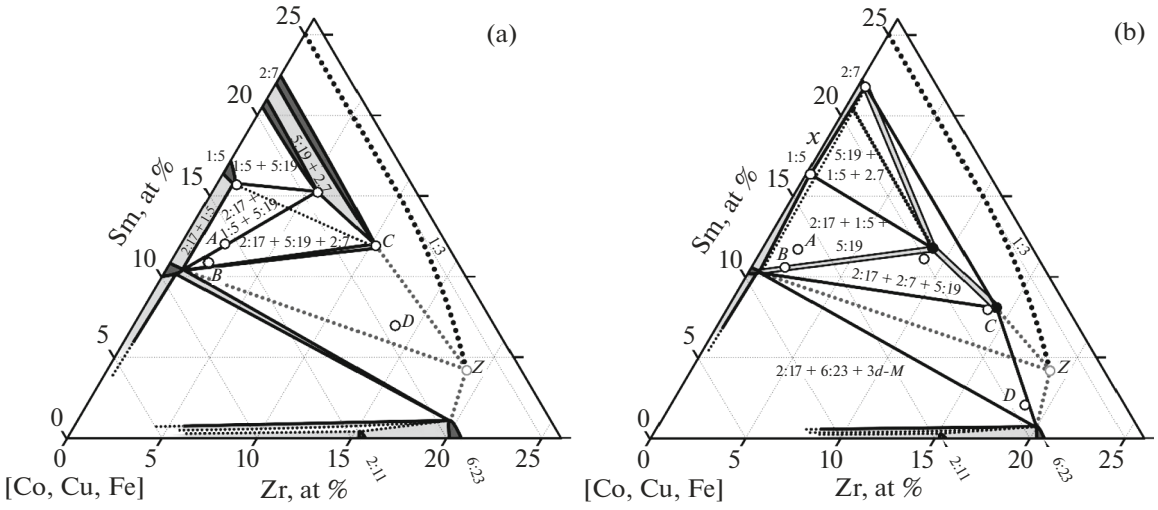

Fig. 5. Visualization of data of electron microprobe analysis on the Sm–Zr–(Co, Cu, Fe) concentration triangle for pseudo-single-crystal (Sm, Zr)(Co, Cu, Fe)$_z$ samples subjected to (a) isothermal aging at 800°C for 20 h and quenching and (b) isothermal treatment at 800°C for 20 h and subsequent stepped aging [14–19].

is confirmed by data of numerous studies, in particular, [31].

Thus, we can state the following.

1. Images given in [28–30] really are not partial sections of the quasi-ternary Sm–Zr–(Co, Cu,Fe) phase diagram but most likely are projections of required sections on the Sm–(Co, Cu, Fe)–T plane.

2. The boundary of high-temperature homogeneity region of the 2:17 phase, which is nearest to the (Co, Cu, Fe) corner of the concentration triangle of the quasi-ternary phase diagram and corresponds to the limit of the (Sm, Zr)$_2$(Co, Cu, Fe)$_{17}$ – H polymorphic modification in the isothermal section at 1160–1185°C, is parallel to the Sm–Zr side of the concentration triangle.

3. The real homogeneity region of the 2:17 phase at 800°C is substantially smaller than that given in [28–30] and corresponds to region *1'* in Fig. 4.

Figure 9 in [14] shows the retrospective review of transformation of isopleth sections of the partial quasi-ternary Sm–Zr–(Co, Cu, Fe) phase diagram with gradual change in the Fe/Cu/Zr ratios according to data of [28–30] after introduction of the corresponding corrections. The retrospective view together with Fig. 4 give a clear view on the giant scale of supersaturation the solid solution based on the 1:7 phase at 800°C after quenching from 1160–1185°C. This supersaturation of the solid solution at low temperatures determines its subsequent decomposition (precipitation strengthening process of alloy) in the course of isothermal aging.

It should be noted that the real supersaturation of the solid solution is substantially higher, and the region of high-temperature solid solution is substantially wider than that given in Fig. 4 in accordance with [28–30].

The fact is that, in [28–30], the structural constituent of the 1:7 phase was related to one of high-temperature polymorphic modifications of 2:17. In turn, we and other investigators assume that, taking into account the unit cell parameters and space group $P6/mmm$, it is correct to consider this constituent as the individual phase that is formed on the basis of the structure of the 1:5 compound and the 2:17 phase adjoint to the boundaries. In [28–30], the region of existence of the 1:7 phase is limited by the solid boundary of the 2:17 phase and, at the same time, is extended with a dashed line almost to the 1:5 stoichiometry (Fig. 4, region *3*). In our opinion, the 1:7 region is extended far beyond the 1:5 phase boundaries toward the 5:19 and 2:7 phases. As the Zr content increases, this region gets a substantial tilt toward the Zr–Sm axis direction near the $SmCo_5$ phase. Owing to the mutual substitution of Sm and Zr in the lattice of intermetallic compounds of the (Sm, Zr)$_{n-1}$Co5$_{n-1}$ homologous series, the Co-to-Sm concentration ratio in the 1:7 phase within this tilted region continues to remain Co/Sm ≥ 5, whereas all change in the stoichiometry occurs through addition of Zr (Figs. 13 and 14 in [14]).

Figure 5 illustrates the result of decomposition of the 1:7 solid solution. The visualization of local microanalysis data for the phases in the pseudo-single crystals of (Sm, Zr)(Co, Cu, Fe)$_z$ samples of experimental series with wide variations of concentration ranges or the ratios of 4*f*-/4*d*-/3*d*-elements is given in the form of partial isothermal sections of the quasi-ternary Sm–Zr–(Co,Cu,Fe) phase diagram.

The structural constituents in Fig. 5 and below are given in designations accepted in [14–19]; i.e., *A* and

B are the main heterophase structural constituents of the pseudo-single-crystal samples, which retain the volume fraction from the solidification to the end of solid solution heat treatment for the high-coercivity state. The *C*, *D*, *E*, and *X* phases are determined on the basis of the results of local microprobe analysis only within structural constituent *A*; the compositions of the phases are 2:7*R*, 6:23, 5:19*R*, 1:5*H*, and 2:7*H*, respectively ([14–19], Fig. 3), and lamellar phase *Z*.

We showed that, in the used objects of study, which are characterized by high hysteretic parameters and major hysteresis loops for samples in the high-coercivity state, which ensure the satisfied condition $(BH)_{max} \approx (4\pi J_S)^2/4$, the 2:7 and 5:19 phases are present in samples quenched after isothermal aging and even in samples subjected to the complete heat treatment cycle including the stepped aging [14–19]. In this case, the (Sm, Zr)(Co, Cu, Fe)$_z$ samples are characterized by the presence of phases almost free of zirconium 2:17 [31] and *X*, that is, $Sm(Co_{0.50–0.63}Cu_{0.22–0.40}Fe_{0.10–0.15})_{3.5–5.0}$, which obviously are the main elements of high-coercivity cellular structure [14–19].

It is noteworthy that these results concerning the presence of the 2:7 and 5:19 phases in the structure of the (Sm, Zr)(Co, Cu, Fe)$_z$ alloys at different heat-treatment stages partially coincide with data of [28–30]. In particular, we showed that the 2:17 and 2:7 phases, on the basis of which structural constituents *B* and *C* form, are the primary solidification phases, which are maximally spaced in the material structure [14–19]; this corresponds to the phase equilibria on images of phase diagrams [28–30], namely, Liq. + 2:17 → Liq. + 2:17 + 2:7. Moreover, the results of the solid solution decomposition in these phase diagrams, at least in a temperature range from 1160–1185 to 1000°C, are the 2:17 + 2:7 phases, and only at lower temperatures does the phase composition of the mixture become 2:17 + 1:5 + 2:7.

In our redaction, the main products of decomposition during isothermal aging are the 2:17 + 2:7 + 5:19 + Z phases and likely some volume fraction of the 1:5 phase.

Thus, the main role of zirconium in the (Sm, Zr)(Co, Cu, Fe)$_z$ permanent magnets consists in the following:

(1) the modification of the phase composition of alloys which ensures the formation of wide regions of continuous solid solutions based on the 1:7 phase (space group *P*6/*mmm*) in the course of high-temperature homogenizing treatment at 1160–1185°C;

(2) the preservation of the structure and supersaturation of this phase at the quenching stage to room temperature; and

(3) the creation of preconditions for the subsequent decomposition of the 1:7 phase (precipitation strengthening of alloy) at the subsequent isothermal aging stage.

In this case, the 5:19, 2:7, and 1:3 phases in the Sm–Zr–Co system, which contain from 5 to 17 at % Zr [32] (in accordance the increase in the Zr content along the 5:19, 2:7, and 1:3 series), are clearly identified also in the structure of five-component magnets but with the wider solubility limits of Zr (from 8.8 to 18.8 at %), which substitutes for Sm.

Role of Copper in (Sm,Zr)(Co,Cu,Fe)$_z$ Alloys

In considering the (Sm, Zr)(Co, Cu, Fe)$_z$-based magnets, K.J. Strnat [2] has recommended to look closely at results of investigations of the ternary Sm–Co–Cu system, in particular, at results obtained by A.J. Perry [33, 34]. K.J. Strnat has reported in his review [3] almost all graphical materials available in [33, 34] related to the Sm–Co–Cu system and highlighted that he obtained the "slightly modified" materials from the authors.

Figure 6a shows a portion of the isothermal section of the Sm–Co–Cu phase diagram at 800°C and portions of the isopleth section $SmCo_5$–$SmCu_5$ (Fig. 6b), which was plotted on the basis of studies of 1:5 diffusion pairs. Both diagrams contain data on the eutectoid transformation of the 1:5 phase and were constructed by us using data given in [2, 33, 34]. The first thing the eye sees in Fig. 6a is the width (along the Co–Sm axis) of the region of solid solutions of the 2:7 phase that includes the coordinates of both the 2:7 phase and the 5:19 phase. Second is the consequence of the effect (already currently accepted) of eutectoid decomposition of the $SmCo_5$ binary phase at 805–815°C on the change in the universally recognized Sm–Co–Cu phase diagram, namely, the appearance of the 2:7–2:5–2:17 three-phase region. This region, as is shown in the partial isopleth section along the 1:5 compound in Fig. 6b, shifts to the low temperatures as the copper concentration increases.

Thus, the V-shaped portion of this region at 800°C, which is denoted by letter A in Fig. 6a, at 600°C should shift, in accordance with the image in Fig. 6b, to the position indicated by arrow and letter B. Where, in this case, should the other part of three-phase 2:7–1:5–2:17 region move?

One should also pay attention to the fact that, according to data of [34], the Cu solubility in the 2:7 phase at 800°C exceeds 30 at %, whereas, according to data of [35], the Cu solubility in the 5:19 phase at 850°C is more than 10 at %.

Figure 7 shows schematically isopleth sections of regions of copper solid solutions in the 2:7, 5:19, and 2:17 phases, which correspond their stoichiometry in the three-component Sm–Co–Cu system. It is seen that the copper solubility curves in the 2:7, 5:19, and 2:17 phases and 1:5 phase demonstrate the opposite tendency of the solubility change with changing copper content.

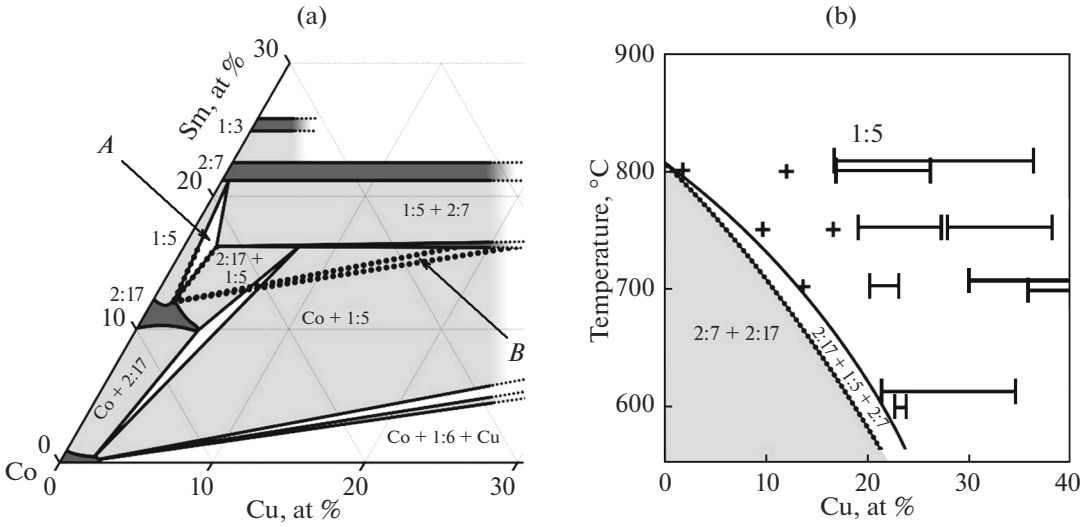

Fig. 6. (a) Portions of isothermal section of the Sm–Co–Cu phase diagram at 800°C and (b) $SmCo_5$–$SmCu_5$ isopleths, data of diffusion pair 1:5 with schematic diagram of eutectoid transformation (plotted according to data cited in [2, 33, 34]).

Iron and zirconium additions to the three-component alloy, the total concentration of which substantially exceeds the copper concentration, should lead to an increase in the eutectoid decomposition temperature of the 1:5 phase substantially above 805–815°C. In this case, the formation of the 2:7 and 5:19 phases during isothermal aging, which are strong acceptors of Zr substituting for Sm in the $(Sm, Zr)_{n-1}(Co, Cu, Fe)_{5n-1}$ phases, seems logical since almost all Zr present in the alloy is forced out into surrounding structural constituents from the formed 2:17*R* phase having a very high volume fraction. In this case, during heat treatment of $(Sm, Zr)(Co, Cu, Fe)_z$ alloys, the phase transformation 2:7 + 5:19 → 1:5 starts if and only if, as a result of diffusion of Cu from the 2:17 phase under aging conditions during slow cooling (or stepped aging), the Cu concentration in the boundary structural constituent "catches up with" the solubility curve of the 1:5 phase, which is ever more going to the $SmCu_5$ composition as the temperature decreases.

It is remarkable that, on the basis of the scheme given in Fig. 7 and taking into account Fig. 6 and the above arguments, it is obvious that the Sm–Co–Cu phase diagram at temperatures below 800°C should take a form qualitatively presented in Fig. 8.

Surprisingly, all available results of studies of the Sm–Co–Cu phase diagram, even those performed a decade after the appearance of permanent magnets based on $(Sm, Zr)(Co, Cu, Fe)_z$ alloys, describe in

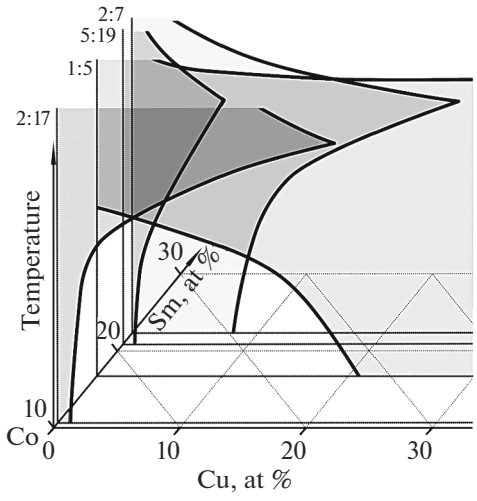

Fig. 7. Schematic diagrams of copper solid solution regions for 2:7, 5:19, 1:5, and 2:17 phases for stoichiometric isopleths of the ternary Sm–Co–Cu system.

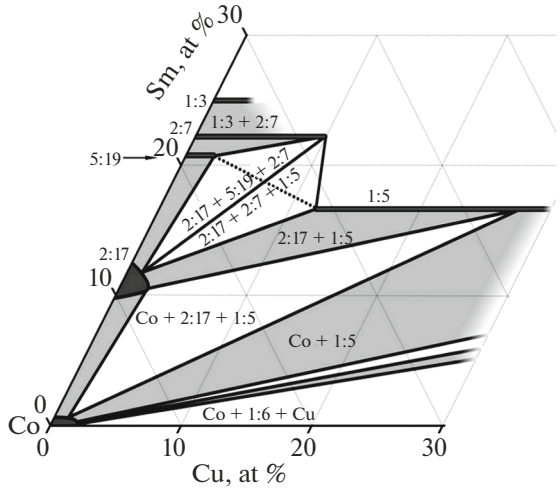

Fig. 8. Qualitative interpretation of the Sm–Co–Cu phase diagram at temperatures below 800°C.

detail the ternary system confined to coordinates Co–$SmCo_5$–$SmCu_5$–Cu at temperatures above 800°C. Nevertheless, the above facts and arguments allow us to assert the following.

(1) The eutectoid decomposition, which, in performing heat treatments "from below," does not allow one to obtain the 1:5 phase in the Sm–Co binary system below 800°C, is an established and generally accepted fact.

(2) Addition of copper decreases the eutectoid transformation temperature in the ternary Sm–Co–Cu system; however, Fe and Zr, which are present in the alloy (Sm, Zr)(Co, Cu, Fe)$_z$ in the total concentration substantially exceeding the Cu content, should abruptly increase the eutectoid decomposition temperature.

(3) Accordingly, the temperature range of isothermal aging of (Sm, Zr)(Co, Cu, Fe)$_z$ alloys is 800–850°C, which is below the eutectoid decomposition temperature of the quinary 1:5 phase and which leads to the formation of a mixture of 5:19 and 2:7 phases between cells since the isothermal aging conditions, in this case, are nothing more than the heat treatment "from below."

(4) Only the proper diffusion saturation of the boundary structural constituent with copper, which is ensured by stepped aging (slow cooling) and is due to curves of variable copper solubility in all phases comprising the system, leads to the formation of the 1:5 phase.

Actually this determines the role of copper in the formation of the structure of the (Sm, Zr)(Co, Cu, Fe)$_z$ alloys in the high-coercivity state.

The interpretation of the Sm–Co–Cu phase diagram, which is shown in Fig. 8, very logically correlates with local electron microprobe analysis data of phases given in the Sm–Zr–(Co, Cu, Fe) concentration triangle for pseudo-single-crystal (Sm, Zr)(Co, Cu, Fe)$_z$ samples (Fig. 2) for the portion of adjacent three-phase 2:17–5:19–2:7–1:5 regions. In turn, the three-phase triangle in Fig. 2 shown at coordinates 2:17–C(2:7)–Z(1:3) likewise corresponds to the similar triangle of the Sm–Co–Fe phase diagram [36].

Peculiarities of Phase Formation in (Sm, Zr)(Co, Cu, Fe)$_z$ Powder Magnets

Researchers have widely recognized the low rate of diffusion processes in the samarium alloys with cobalt and the fact that, at the same temperatures, the diffusion in different phases is different; for example, the diffusion rates of elements in the 2:17 phase is markedly lower than that in the 1:5 phase [34].

In real permanent magnets based on the (Sm, Zr)(Co, Cu, Fe)$_z$ alloys manufactured by powder metallurgy, the effect of different diffusion rates is less substantial owing to the highly refined structure of the material. The homogenization of the material occurs in several stages, beginning in the course of preparation of fine micron powders (through the most high-temperature processes, namely, sintering and supersaturated solid solution treatment) and ending upon the quenching of blanks. Owing to the efficient homogenization, the sintered magnets subjected to the complete heat treatment cycle for the high-coercivity state, in contrast to objects used in the present study, namely, cast pseudo-single-crystal samples, are free of residual structural constituents given in Fig. 2b, namely, C(2:7) and E(5:19), and the lamellar Z phase develops instead of the D(6:23) phase.

In this case, the main structural constituents determining the hysteretic properties of magnets, namely, the 2:17 cellular phase and boundary phase, the composition of which is similar to that of the X phase (Fig. 2, $Sm(Co_{0.50–0.63}Cu_{0.22–0.40}Fe_{0.10–0.15})_{3.5–5.0} \equiv 1{:}5H + 2{:}7H$), in course of prolonged heat treatment, force out almost all Zr into the lamellar Z phase. The boundary phase is likely mainly represented by the 1:5 stoichiometry in ternary junctions of cells as the fraction of 3*d* elements decreases up to the 2:7 composition.

Figure 9 shows, for different stages of heat treatment, the scheme of transformation of the boundary structural constituent for an ideal cell of the structure of a (Sm, Zr)(Co, Cu, Fe)$_z$ permanent magnet manufactured by powder technology.

In the course of stepped aging (slow cooling), the boundary structural constituent (as compared to the boundary structural constituent reached after isothermal aging) transforms from the 2:7 + 5:19 phase mixture into almost Zr-free Cu-enriched phase with markedly decreased width and very level interphase boundaries.

The formation of the high-coercivity structure of a (Sm, Zr)(Co, Cu, Fe)$_z$-based permanent magnet in the course of complete heat treatments cycle (described above) can be represented in the form of the scheme given in Fig. 10.

Some Arguments for Supporters of the Solid Solution Decomposition Based on the 1:7 $\rightarrow$ 2:17 + 1:5 + 1:3 Transformation

Let us consider one of the fundamental studies which are represented as evidence of the simplified model of the formation of the high-coercivity structure of (Sm, Zr)(Co, Cu, Fe)$_z$ alloys in substantiating the direct decomposition reaction 1:7 $\rightarrow$ 2:17 + 1:5 + 1:3 [31].

As the instrumentation methodological support of the obtained results, the authors of [31] have used the 3DAP analysis of phases in a powder magnet, which is characterized by record nanometer resolution. Thus, there is no doubt as to the objectivity of results obtained. However, the high instrumental resolution

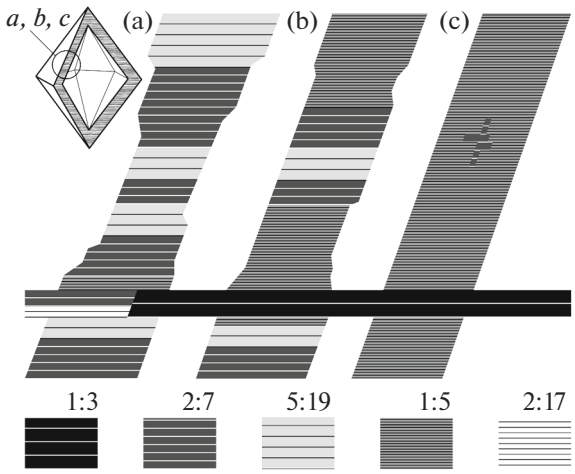

Fig. 9. Schematic diagram of transformations of boundary structural constituent of an ideal structural cell at different stages of heat treatment of a (Sm, Zr)(Co, Cu, Fe)$_z$ permanent magnet manufactured by powder technology. The cell phase 2:17*R* is not shown. Structure of boundary (a) after isothermal aging, (b) in the course of stepped aging (slow cooling), and (c) after heat treatment for the high-coercivity state.

of the method does not ensure the objectivity of choice of the localization of studied microvolumes in samples, since the probability of randomness is high. Moreover, errors in choosing the composition features and technological parameters of preparation of samples are not excluded.

The alloy with a composition of $Sm(Co_{0.72}Fe_{0.20}Cu_{0.055}Zr_{0.025})_{5.7} \equiv (Sm_{0.84}Zr_{0.16})$-$(Co_{0.74}Cu_{0.06}Fe_{0.21})_{6.16}$ used in [29], in accordance with regularities described above on the basis of studies of a number of experimental series, which cover a wide composition range and are described in detail in [14–19], belong to compositions characterized by predominance of volume fraction of the main structural constituent A over that of constituent B. Thus, after optimum treatment for the high-coercivity state, this alloy should demonstrate (a) rather ordinary values of saturation magnetization (remanence) and coercive force, (b) almost zero coercivity after isothermal treatment without stepped aging, and (c) very high hysteresis loop squareness. The saturation magnetization and hysteresis loop squareness are not reported in [29], whereas the other parameters correspond to those given above. The isothermal annealing of samples at 820°C was performed only for 6 h. Therefore, after isothermal aging, the structure of the alloy should show the cellular structure morphology with very narrow interlayers of boundary phase between cells; this was demonstrated by the authors.

Figure 7 in [29] shows the two-coordinate concentration map of copper, with a scale ruler of 2 nm, in the sample quenched from 520°C, which indicates that the width of the profile of increased copper concentration at the boundary phase is no more than ~3 nm. In turn, in Fig. 6b in [29], with results of 3DAP analysis (on a nanometer scale) of cell phase and boundary phase, the width of the boundary phase, which is denoted as $SmCo_5$, is only 1.5 nm, whereas the maximum width of copper concentration profile is 2.5 nm.

It is known that efficient domain wall pinning at structural microelements is possible in the case of continuity (or quasi-continuity) of these elements. The second necessary condition is the fact that the width of these microelements should exceed the domain wall width. According to data of D. Goll et al. [3] for similar magnets, the domain wall width is 5.7 nm within the cell phase and 3.1 nm within the cell boundary (boundary phase). The authors do not consider how the boundary phase only 1.5 nm in width can ensure the effective pinning and the coercive force $H_{CJ} \approx 13$ kOe [29].

In this case, we have every reason to believe that the saturation with copper of the majority of the volume of the boundary phase at its width of ~1.5 nm occurs even at high cooling rates of the sample after isothermal aging. For a different degree of solid solution supersaturation, to reach the quenching effect, there is a minimum limit of the cooling rate of the sample material. For example, an incomplete quenching effect is possible; in this case, a significant but incomplete volume of 2:7 + 5:19 phase mixture within the boundary structural constituent transforms into the 1:5 structure. This variant is shown in Fig. 6b. The incomplete phase transformation leads to alternation of 1:5 phase areas and areas with residues of the mixture of the 2:7 and 5:19 phases along cell boundaries. This is due to the morphology of boundary structure with alternation of phase layers arranged along the basal plane of anisotropic solid mass.

This alternation largely will depend on the distance between the area and ternary junctions of cells and the width of the boundary constituent. In any case, such a boundary structure is fraught with numerous domain wall penetrations, i.e., the low coercive force of samples. This assumption followed from the fact expressed by the authors of [29]. Since for the complete phase transformation 2:7 + 5:19 $\rightarrow$ 1:5 of such a narrow boundary, the stepped aging temperature range shortened to 820–520°C is required, whereas the common temperature of the end of stepped aging is 400°C.

The objectivity of results of 3DAP analysis and the peculiarities of concentration profiles of components of the quinary Sm–Zr–Co–Cu–Fe system in the high-coercivity state, which for the first time were shown in [29], are not in doubt. However, we should

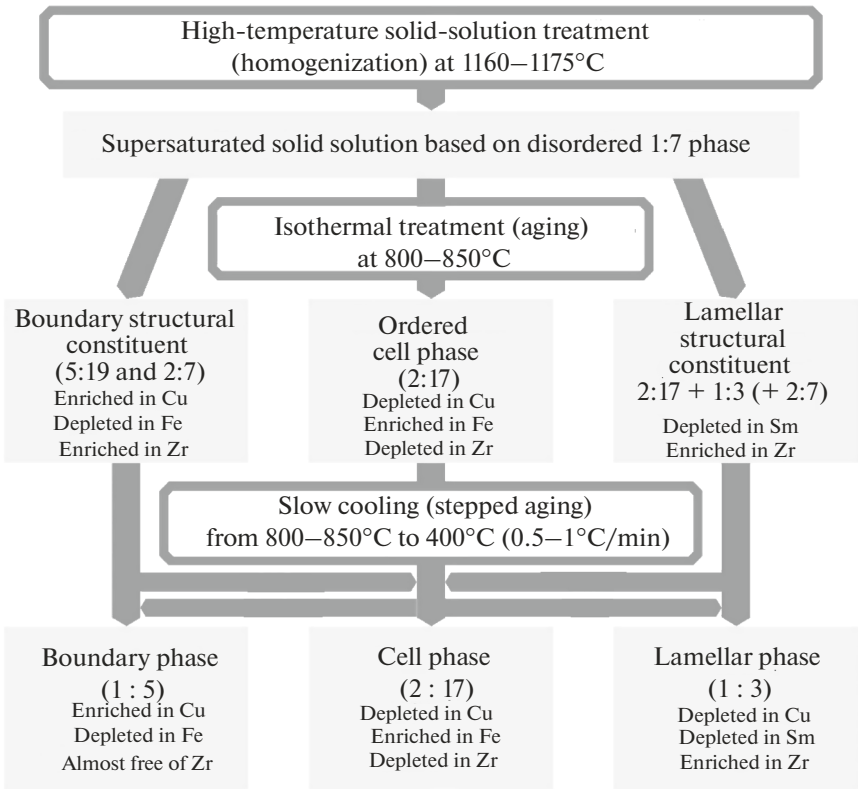

Fig. 10. Block diagram of the mechanism of structure formation of high-coercivity state of a (Sm,Zr)(Co,Cu,Fe)$_z$ permanent magnet in the course of complex heat treatment.

agree that the particular case considered in [29] is a weak argument in favor of generalizations made from the particular case.

CONCLUSIONS

The processes of structure formation of cast magnetically uniaxial samples of (Sm, Zr)(Co, Cu, Fe)$_z$ alloys for permanent magnets are studied for wide ranges of concentrations and relationships of 4*f*-/4*d*-/3*d*-elements comprising them, namely, for the $Sm_{0.95–0.07}5Zr_{0.05–0.025}(Co_{bal}Cu_{0.075–0.088}Fe_{0.260–0210})_{5.5–7.0}$ compositions. On the basis of the analysis, comparison, and generalization of results obtained in studying the structure and hysteretic characteristics of samples corresponding to specific stages of complex heat treatment with application of various methods of physical metallurgy, the model of formation of the high-coercivity state of (Sm,Zr)(Co,Cu,Fe)$_z$ alloys for permanent magnets was revised.

FUNDING

This study was supported by the Russian Science Foundation, project no. 20-19-00689, "Development of the Model of Formation of High-Coercivity Phase and Structural States of (R, Zr)(Co, Cu, Fe)$_z$ Alloys and Synthesis of Them for Manufacturing Anisotropic Bonded Powder Permanent Magnets Applied in Electric Machines."

CONFLICT OF INTEREST

The authors of this work declare that they have no conflicts of interest.

REFERENCES

1. Coey, J.M.D., Perspective and prospects for rare earth permanent magnets, *Engineering,* 2020, vol. 6, no. 2, pp. 119–131. https://doi.org/10.1016/j.eng.2018.11.034
2. Strnat, K.J., Rare earth-cobalt permanent magnets, in *Handbook of Ferromagnetic Materials,* Wohlfarthf, E.P. and Buschow, K.H.J., Eds., Elsevier, 1988, vol. 4, pp. 131–209. https://doi.org/10.1016/S1574-9304(05)80077-X
3. Goll, D., Kronmüller, H., and Stadelmaier, H.H., Micromagnetism and the microstructure of high-temperature permanent magnets, *J. Appl. Phys.,* 2004, vol. 96, pp. 6534–6545. https://doi.org/10.1063/1.1809250
4. Sepehri-Amin, H., Thielsch, J., Fischbacher, J., Ohkubo, T., Schrefl, T., Gutfleisch, O., and Hono, K., Correlation of microchemistry of cell boundary phase and interface structure to the coercivity of

$Sm(Co_{0.784}Fe_{0.100}Cu_{0.088}Zr_{0.028})_{7.19}$ sintered magnets, *Acta Mater.*, 2017, vol. 126, pp. 1–10. https://doi.org/10.1016/j.actamat.2016.12.050

5. Gopalan, R., Ohkubo, T., and Hono, K., Identification of the cell boundary phase in the isothermally aged commercial $Sm(Co_{0.725}Fe_{0.1}Cu_{0.12}Zr_{0.04})_{7.4}$ sintered magnet, *Scr. Mater.,* 2006, vol. 54, no. 7, pp. 1345–1349. https://doi.org/10.1016/j.scriptamat.2005.12.009
6. Zhang, Y., Tang, W., Hadjipanayis, G.C., Chen, C., Nelson, C., and Krishnan, K., Evolution of microstructure, microchemistry and coercivity in 2:17 type Sm–Co magnets with heat treatment, *IEEE Trans. Magn.,* 2001, vol. 37, no. 4, pp. 2525–2527. https://doi.org/10.1109/20.951223
7. Ray, A.E., A revised model for the metallurgical behavior of 2:17-type permanent magnet alloys, *J. Appl. Phys.,* 1990, vol. 67, no. 9, pp. 4972–4074. https://doi.org/10.1063/1.344720
8. Kronmuller, H. and Goll, D., Micromagnetic analysis of pinning-hardened nanostructured, nanocrystalline Sm_2Co_{17} based alloys, *Scr. Mater.,* 2002, vol. 47, no. 8, pp. 545–550. https://doi.org/10.1016/S1359-6462(02)00177-X
9. Stadelmaier, H.H., Goll, D., and Kronmuller, H., Permanent magnet alloys based on Sm_2Co_{17}; phase evolution in the quinary system Sm–Zr–Fe–Co–Cu, *Z. Metallkd.,* 2005, vol. 96, no. 1, pp. 17–23. https://doi.org/10.3139/146.018078
10. Goll, D., Stadelmaier, H.H., and Kronmuller, H., Samarium–cobalt 2:17 magnets: Analysis of the coercive field of $Sm_2(CoFeCuZr)_{17}$ high-temperature permanent magnets, *Scr. Mater.,* 2010, vol. 63, no. 2, pp. 243–245. https://doi.org/10.1016/j.scriptamat.2010.03.066
11. Stadelmaier, H.H., Kronmuller, H., and Goll, D., Samarium–cobalt 2:17 magnets: Identifying $Sm_{n+1}Co_{5n-1}$ phases stabilized by Zr, *Scr. Mater.,* 2010, vol. 63, no. 8, pp. 843–846. https://doi.org/10.1016/j.scriptamat.2010.06.033
12. Song, K., Sun, W., Chen, H., Yu, N., Fang, Y., Zhu, M., and Li, W., Revealing on metallurgical behavior of iron-rich $Sm(Co_{0.65}Fe_{0.26}Cu_{0.07}Zr_{0.02})_{7.8}$ sintered magnets, *AIP Adv.,* 2017, vol. 7, no. 5, p. 056238. https://doi.org/10.1063/1.4978464
13. Song, K., Fang, Y., Wang, S., Yu, N., Chen, H., Zhang, M., Zhu, M., and Li, W., Crystalline and magnetic microstructures of iron-rich $Sm(Co_{0.65}Fe_{0.26}Cu_{0.07}Zr_{0.02})_{7.8}$ sintered magnets: Isothermal aging effect, *J. Magn. Magn. Mater.,* 2018, vol. 465, pp. 569–577. https://doi.org/10.1016/j.jmmm.2018.06.047
14. Dormidontov, A.G., Kolchugina, N.B., Dormidontov, N.A., and Milov, Yu.V., Structure of alloys for $(Sm,Zr)(Co,Cu,Fe)_z$ permanent magnets: First level of heterogeneity, *Materials,* 2020, vol. 13, no. 17, p. 3893. https://doi.org/10.3390/ma13173893
15. Dormidontov, A.G., Kolchugina, N.B., Dormidontov, N.A., Milov, Yu.V., and Andreenko, A.S., Structure of alloys for $(Sm, Zr)(Co, Cu, Fe)_z$ permanent magnets: II. Composition, magnetization reversal, and magnetic hardening of main structural components, *Materials,* 2020, vol. 13, no. 23, p. 5426. https://doi.org/10.3390/ma13235426
16. Dormidontov, N.A., Kolchugina, N.B., Milov, Yu.V., and Dormidontov, A.G., Peculiarities of the formation of high-coercivity structure of $(Sm,Zr)(Co,Cu,Fe)_z$ alloys in varying the (4*f*-, 4*d*-)-to-(3*d*-) element ratio, *Inorg. Mater.: Appl. Res.,* 2021, vol. 12, no. 2, pp. 491–498. https://doi.org/10.1134/S2075113321020118
17. Dormidontov, A.G., Kolchugina, N.B., Dormidontov, N.A., Zheleznyi, M.V., Bakulina, A.S., Prokofev, P.A., Andreenko, A.S., Milov, Yu.V., and Sysoev, N.N., Structure of alloys for $(Sm, Zr)(Co, Cu, Fe)_z$ permanent magnets: III. Matrix and phases of the high-coercivity state, *Materials,* 2021, vol. 14, no. 24, p. 7762. https://doi.org/10.3390/ma14247762
18. Dormidontov, N.A., Kolchugina, N.B., Prokof'ev, P.A., Zheleznyi, M.V., Milov, Yu.V., Dormidontov, A.G., and Bakulina, A.S., Structural constituents and phases in highcoercivity $(Sm, Zr)(Co, Cu, Fe)_z$ alloys for permanent magnets, *Russ. Metall. (Metally),* 2022, vol. 2022, no. 5, pp. 505–511. https://doi.org/10.1134/S0036029522050032
19. Zheleznyi, M.V., Kolchugina, N.B., Dormidontov, N.A., Prokofev, P.A., Milov, Yu.V., Sipin, I.A., Andreenko, A.S., Dormidontov, A.G., and Bakulina, A.S., Structure of alloys for $(Sm, Zr)(Co, Cu, Fe)_z$ permanent magnets: Phase composition of as-cast alloys, *Russ. Metall. (Metally),* 2022, vol. 2022, no. 11, pp. 1464–1468. https://doi.org/10.1134/S0036029522110192
20. Perkins, R.S. and Strassler, S., Interpretation of the magnetic properties of pseudobinary $Sm_2(Co, M)_{17}$ compounds. I. Magnetocrystalline anisotropy, *Phys. Rev. B*, 1977, vol. 15, no. 1, pp. 477–489.
21. Perkins, R.S. and Strassler, S., Interpretation of the magnetic properties of pseudobinary $Sm_2(Co, M)_{17}$ compounds. II. Magnetization, *Phys. Rev. B,* 1977, vol. 15, no. 1, pp. 490–495.
22. Fujii, H., Satyanarayana, M.V., and Wallace, W.E., Effect of substitution of Zr on the magnetic properties of R_2Co_{17} (R = Ce and Sm), *Solid State Commun.,* 1982, vol. 41, no. 6, pp. 445–448.
23. Nishio, T., Fukui, Y., and Iwama, Y., Effect of zirconium on stabilization for the 1-7 phase in 2-17 type Sm–Co permanent magnet, *J. Jpn. Inst. Met.,* 1988, vol. 52, no. 5, pp. 502–507. https://doi.org/10.2320/jinstmet1952.52.5_502
24. Derkaoui, S., Valignat, N., and Allibert, C.H., Co corner of the system Sm–Co–Zr: Decomposition of the phase 1:7 and equilibria at 850°C, *J. Alloys Compd.,* 1996, vol. 235, pp. 112–119.
25. Derkaoui, S., Valignat, N., and Allibert, C.H., Phase equilibria at 1150°C in the Co-rich alloys Sm–Co–Zr and structure of the 1:7 phase, *J. Alloys Compd.,* 1996, vol. 232, pp. 296–301.
26. Lefevre, A., Cataldo, L., Cohen-Adad, M.Th., Allibert, C.H., and Valignat, N., The ternary system Sm–Co–Zr isoplethic section at Co = 89 at %, *J. Alloys Compd.,* 1996, vol. 241, pp. 210–215.
27. Lefevre, A., Cataldo, L., Cohen-Adad, M.Th., and Mentzen, B.F., The ternary system Sm–Co–Zr isople-

thic sections at Co = 87 and 85 at %, *J. Alloys Compd.,* 1997, vol. 255, pp. 161–168.

28. Morita, Y., Umeda, T., and Kimura, Y., Phase transformation at high temperatures and coercivity of Sm–Co–Cu–Fe magnet alloys, *J. Jpn. Inst. Met.,* 1986, vol. 50, no. 5, pp. 235–241.
29. Morita, Y., Umeda, T., and Kimura, Y., Phase transformation at high temperature and coercivity of Sm(Co, Cu, Fe, Zr)$_{7–9}$ magnet alloys, *IEEE Trans. Magn.,* 1987, vol. 23, pp. 2702–2704.
30. Morita, Y., Umeda, T., and Kimura, Y., Effects of Zr content on phase transformation and magnetic properties of Sm(Co, Cu, Fe, Zr)$_{7–9}$ magnet alloys, *J. Jpn. Inst. Met.,* 1988, vol. 52, pp. 243–250, 26–28.
31. Xiong, X.Y., Ohkubo, T., Koyama, T., Ohashi, K., Tawara, Y., and Hono, K., The microstructure of sintered Sm $(Co_{0.72}Fe_{0.20}Cu_{0.055}Zr_{0.025})_{7.5}$ permanent magnet studied by atom probe, *Acta Mater.,* 2004, vol. 52, no. 3, pp. 737–748. https://doi.org/10.1016/j.actamat.2003.10.015
32. Derkaoui, S., Valignat, N., and Allibert, C.H., Co corner of the system Sm–Co–Zr: Decomposition of the phase 1:7 and equilibria at 850°C, *J. Alloys Compd.,* 1996, vol. 235, pp. 112–119.
33. Perry, A.J., The eutectoid transformation of Sm(Co,Cu)$_5$, *IEEE Trans. Magn.,* 1976, vol. 12, pp. 962–964.
34. Perry, A.J., The constitution of copper-hardened samarium-cobalt permanent magnets, *J. Less-Common Met.,* 1977, vol. 51, pp. 153–162.
35. Derkaoui, S. and Allibert, C.H., Redetermination of the phase equilibria in the system Sm–Co–Cu for Sm content 0–20 at % at 850°C, *J. Less-Common Met.,* 1989, vol. 154, pp. 309–315.
36. Schneider, G., Henig, E.-Th., Lucas, H.L., and Petzov, G., Phase relations in the samarium-poor Sm–Co–Fe system, *J. Less-Common Met.,* 1985, vol. 110, pp. 159–170.

Translated by N. Kolchugina